

Design Considerations for a Ground-based Transit Search for Habitable Planets Orbiting M dwarfs

Philip Nutzman and David Charbonneau ¹

Harvard-Smithsonian Center for Astrophysics, 60 Garden St., Cambridge, MA 02138

pnutzman@cfa.harvard.edu

ABSTRACT

By targeting nearby M dwarfs, a transit search using modest equipment is capable of discovering planets as small as $2 R_{\oplus}$ in the habitable zones of their host stars. The MEarth Project, a future transit search, aims to employ a network of ground-based robotic telescopes to monitor M dwarfs in the northern hemisphere with sufficient precision and cadence to detect such planets. Here we investigate the design requirements for the MEarth Project. We evaluate the optimal band-pass, and the necessary field of view, telescope aperture, and telescope time allocation on a star-by-star basis, as is possible for the well-characterized nearby M dwarfs. Through these considerations, 1,976 late M dwarfs ($R < 0.33 R_{\odot}$) emerge as favorable targets for transit monitoring. Based on an observational cadence and on total telescope time allocation tailored to recover 90 % of transit signals from planets in habitable zone orbits, we find that a network of ten 30 cm telescopes could survey these 1,976 M dwarfs in less than 3 years. A null result from this survey would set an upper limit (at 99 % confidence) of 17 % for the rate of occurrence of planets larger than $2 R_{\oplus}$ in the habitable zones of late M dwarfs, and even stronger constraints for planets lying closer than the habitable zone. If the true occurrence rate of habitable planets is 10 %, the expected yield would be 2.6 planets.

Subject headings: stars: low mass — stars: planetary systems — techniques: photometric — surveys — extrasolar planets

¹Alfred P. Sloan Research Fellow

1. Introduction

In upcoming years, the study and characterization of exoplanets will depend largely on the unique window that transiting planets offer into their properties. Transit observations reveal a planet’s radius, and in combination with radial-velocity measurements, permit a determination of the planet’s mass. This combination of measurements provides the only available direct constraint on the density and hence bulk composition of exoplanets. When a planet cannot be spatially resolved from its host star, transit-related observations typically offer the only means for direct measurements of planetary emission and absorption. Already, transmission spectroscopy has probed the atmospheric chemistries of HD 209458b (Charbonneau et al. 2002; Vidal-Madjar et al. 2003; Barman 2007) and HD 189733b (Tinetti et al. 2007), while infrared monitoring during secondary eclipse has led to the detection of broadband thermal emission from HD 209458b, TrES-1, HD 189733b, HD 149026b, and GJ 436b (Deming et al. 2005; Charbonneau et al. 2005; Deming et al. 2006; Harrington et al. 2007; Deming et al. 2007). Precise spectroscopic measurements during secondary eclipse have unveiled the infrared spectrum of HD 209458b (Richardson et al. 2007), and HD 189733b (Grillmair et al. 2007). Most recently, infrared observations gathered at a variety of orbital phases have allowed the characterization of the longitudinal temperature profiles for several Hot Jupiters (Harrington et al. 2006; Knutson et al. 2007; Cowan et al. 2007). These and a host of other studies (as reviewed by Charbonneau et al. 2007) demonstrate the profound impact of the transiting class of exoplanets.

Given the importance of the transiting planets, it is critical to extend their numbers to planets in different mass regimes, different irradiation environments, and around varied star types. Until the recent discovery that the Neptune-sized GJ 436b transits its host M dwarf (Gillon et al. 2007), all known transiting planets were hot gas giants orbiting Sun-like stars. A discovery like this points to the advantages that M dwarfs provide for expanding the diversity of the transiting planets; the advantages are particularly acute for the detection of rocky, habitable planets (see e.g. Gould et al. 2003). We review these observational opportunities by explicitly considering the case of a $2 R_{\oplus}$ planet (representing the upper end of the expected radius range for super-Earths, see Valencia et al. 2007 and Seager et al. 2007) orbiting in the habitable zones of the Sun and a fiducial M5 dwarf ($0.25 M_{\odot}$, $0.25 R_{\odot}$, $0.0055 L_{\odot}$).

1. The habitable zones of M dwarfs are drawn in close to the stars, improving the transit likelihood. A planet receiving the same stellar flux as the Earth would lie only 0.074 AU from the M5, and would present a 1.6 % geometric probability of transiting, compared to the 0.5 % probability for the Earth-Sun system. Note that here, and throughout the paper, we define habitable zone orbits to be at the orbital distance for which the planet receives the same insolation flux as the Earth receives from the Sun.

2. Transits from the habitable zones of M dwarfs happen much more frequently. At 0.074 AU from the M5, a planet would transit once every 14.5 days, compared to 1 year for the Earth-Sun system. This is critical for detectability, as dramatically less observational time is required to achieve a transit detection.
3. The small radii of M dwarfs lead to much deeper transits. The $2-R_{\oplus}$ planet would eclipse 0.5 % of an M5’s stellar disk area, but only 1 part in 3000 of that of the Sun.
4. The small masses of M dwarfs lead to larger induced radial velocity variations. Taking a mass of $7 M_{\oplus}$ for the super-Earth (in a habitable zone orbit with $P=14.5$ days), the induced peak-to-peak velocity variation on the M5 is 10 m/s, versus an induced 1.3 m/s variation at 1 AU from the Sun.

A transit survey targeting nearby, proper motion selected M dwarfs would also avoid a number of astrophysical false alarms (see e.g. Mandushev et al. 2005 and O’Donovan et al. 2006). Among the most common false alarms are those caused by eclipsed giant stars, hierarchical triples composed of a star plus an eclipsing pair, grazing eclipsing binaries, and blends with fainter background eclipsing binaries. The survey would avoid eclipsed giant stars by construction; a giant would never be confused as a nearby, high proper motion M dwarf. Hierarchical triple systems would be exceedingly unlikely, given the red colors and low intrinsic luminosity of the system. In any case, given its proximity, such a system would likely be partially resolvable through high-resolution imaging. Grazing eclipsing binaries would also be unlikely, though interesting, given the rarity of double M dwarf eclipsing pairs. A spectroscopic study looking for the presence of double lines could easily confirm or rule out this scenario. Blends with background binaries are, in principle, still an issue for a targeted M dwarf survey. However, because of the high proper motions of the M dwarfs, chance alignments could be confirmed or ruled out with archived or future high resolution observations.

Aside from these observational advantages, several developments in astrophysics point to exciting possibilities with M dwarfs. Firstly, the growing number of M dwarf exoplanet discoveries, including the $\sim 5.5-M_{\oplus}$ planet orbiting Gliese 581c (Udry et al. 2007) and the microlensing discovery OGLE 2005-BLG-390Lb (Beaulieu et al. 2006), suggest an abundance of *sub*-Neptune mass planets orbiting M dwarfs. It is an open challenge to find a transiting planet in this mass regime; simply obtaining a radius measurement for such a planet (for which there are no Solar System analogs) would be extremely fruitful as it might allow one to distinguish between rocky or ocean planet composition models (Valencia et al. 2007). Intriguingly, the idea that life can survive on habitable zone planets around M dwarfs has been recently rehabilitated (see Scalo et al. 2007 and Tarter et al. 2007 for detailed discussion) . Previously, it had been assumed that the rotational synchronization expected of

close-in habitable zone planets would lead either to atmospheric collapse or to steep temperature gradients and climatic conditions not suitable for life. Works reviewed in Scalo et al. and Tarter et al. argue that atmospheric heat circulation should prevent each of these barriers to habitability. Regardless, the absence of such heat redistribution would be readily observable with precise infrared photometric monitoring as a large day-night temperature difference, while the detection of a small day-night difference would provide a strong case for the existence of a thick atmosphere.

With Spitzer and the James Webb Space Telescope (JWST), atmospheric observations similar to those mentioned earlier for Hot Jupiters can be extended to habitable, Earth-sized planets orbiting M dwarfs. This possibility is brought about by the small surface areas and temperatures of M dwarfs, which lead to significantly more favorable planet-star contrast ratios. This ratio for a habitable $2-R_{\oplus}$ planet orbiting an M5 is 0.05 % (in the Rayleigh-Jeans limit), leading to secondary eclipse depths well reachable with Spitzer’s sensitivity (this compared to a contrast ratio 0.0017 % for a habitable $2-R_{\oplus}$ orbiting the Sun). JWST photometry will be capable of measuring the day-night temperature difference for warm Earth-like planets orbiting M dwarfs (Charbonneau & Deming 2007), thus addressing the extent of heat redistribution on these planets and hence the presence or absence of an atmosphere.

It is interesting to consider the place of M dwarf planets in the expected yields of ongoing and upcoming transit surveys. The COROT (Baglin 2003) and Kepler (Borucki et al. 2003) space missions are the most ambitious of the transit surveys; with long, uninterrupted time baselines and excellent photometric precision, these missions should yield rocky planets with orbital periods much longer than those detected by ground-based transit searches. Gould et al. (2003) point out that missions like COROT and Kepler are much more sensitive to M dwarf habitable planets than to solar-type habitable planets, if they can be reliably monitor the M dwarfs to faint magnitudes ($V > 17$). In practice, stellar crowding, noise from sky background, and other technical issues (Gould et al. 2003; Deeg 2004) strongly limit their sensitivity to these faint magnitudes. COROT and Kepler can precisely monitor bright, nearby M dwarfs, but with Kepler observing one fixed field of roughly 100 square degrees, and COROT monitoring much less sky area, these missions probe only a small number of such nearby M dwarfs. Wide-angle ground surveys, such as HATNet (Bakos et al. 2004), SuperWASP (Pollacco et al. 2006), TrES (Alonso et al. 2004), and XO (McCullough et al. 2005) cumulatively cover swaths of sky containing large numbers of nearby M dwarfs, but at the expense of employing apertures too modest to effectively probe any but the brightest of these M dwarfs (see e.g. McCullough & Burke 2007).

Motivated by these difficulties, and the fact that the closest, most observationally favor-

able M dwarfs are spread sparsely throughout the sky, we consider an alternative approach in which these M dwarfs are *individually* targeted. In this paper, we develop a concept that we term the MEarth Project, which envisions a cluster of robotic telescopes dedicated to targeted, sequential photometric monitoring of nearby M dwarfs. We determine the necessary design elements for a survey searching for transiting planets as small as $2 R_{\oplus}$ (the upper end of the rocky planet regime), and out to the M dwarf habitable zones. In §2, we briefly discuss the MEarth Project concept. In §3 we describe already compiled lists of nearby M dwarfs suitable for observations. We discuss their observational properties and use these to estimate basic stellar parameters. In §4 we determine the necessary telescope aperture through a calculation that estimates the photometric precision for M dwarf stars. In §5 we determine the necessary field of view, which is driven by the need for a sufficient number of calibrator stars. In §6 we estimate the amount of gross telescope time necessary for a successful survey for an optimal list of late M dwarf targets for the MEarth project. In §7 we wrap up with a discussion of our conclusions and the design implications for the MEarth project.

2. MEarth Project: Discussion

The heart of the MEarth concept is to use a network of robotic telescopes to precisely monitor the brightness of roughly 2000 northern, nearby M dwarfs, with a sensitivity sufficient to detect $2\text{-}R_{\oplus}$ planets. The MEarth network will be housed in a single enclosure on Mt. Hopkins, Arizona. Multiple sites spread in longitude would be observationally favorable, but would unfortunately be a cost-prohibitive arrangement. The number of targets is selected to ensure that even a null result is astrophysically interesting, while the sensitivity goal reaches into the upper end of the radius range expected for rocky planets. If we take the fiducial M5V star as typical of the M dwarfs being monitored, and assume an occurrence rate of 10 % for habitable zone planets larger than $2 R_{\oplus}$, the expected yield from 2000 M dwarfs is 3.2 planets, which would complement Kepler’s expected harvest of habitable planets around Sun-like stars (Gillon et al. 2005). Correspondingly, a null result places an upper limit for the occurrence rate of such habitable planets at 15 % (at 99 % confidence). Note that later we will refine this calculation using actual estimates of R_{\star} and a_{HZ} for 1,976 observationally favorable M dwarf targets.

Perhaps the most critical aspect of the MEarth project is that the M dwarfs are observed one-by-one. This sequential mode of observing comes with a certain benefit: the field of view requirements are relaxed and set only by the need for the field to contain a sufficient number of comparison stars (see §5). A modest field of view requirement opens up the possibility

of using off-the-shelf equipment and dodges many of the technical challenges that beset wide-field transit searches (see e.g. Bakos et al. 2004 and McCullough & Burke 2007 for a discussion of these issues).

On the other hand, the observational cadence achieved per target when sequentially targeting M dwarfs is significantly less than when staring at and repeatedly imaging a single field. There are two issues which help compensate for the sparse cadence. Firstly, typical levels and timescales of correlated noise in photometric surveys (see e.g. Pont et al. 2006) suppress the benefit of dense time sampling such that the ‘standard’ $N^{-1/2}$ improvement in precision generally does not apply. Secondly, the flexibility of being able to choose your targets and when to observe them greatly enhances the efficiency per observation of the transit survey. We envision an adaptively scheduled transit search, wherein the observing sequence is updated as the images are gathered and analyzed. We consider a design in which transits are identified while in progress by the automated reduction software. The subsequent alert triggers other telescopes in the MEarth array (or at another observatory) for high-cadence monitoring at improved precision and in multiple colors until a time after transit egress. Intense coverage following this could then pin down the orbital period. Under this observing strategy, the amount of time required to achieve detection is the amount of time until the first transit event falls during an observation session. This is significantly less time than is required for current transit surveys, which spot transits in phase-folded archived data and typically require at least 3 distinct transit events.

Note that in this adaptive mode of observing, a false positive triggered by photometric noise is addressed immediately and, in most cases, easily dismissed with a few additional exposures. False positives, in this context, are thus far less costly than in traditional transit surveys. This, coupled with the fact that the MEarth network will monitor only a couple hundred M dwarfs on any given night, means that the follow-up mode can be triggered at a relatively low statistical threshold. In our paper, we require a per-point photometric precision that is three times smaller than the given transit depth of interest. A threshold near ‘3 sigma’ would be outlandish for a traditional transit survey monitoring hundreds of thousands of stars, but here would lead to an inexpensive fraction of time spent on false alarms each night. It is important to note that while follow-up is triggered at relatively low significance, a genuine transit would be detected by MEarth to higher significance, as the entire MEarth network would be galvanized to high-cadence follow-up.

The level of significance of this transit detection would depend on the transit depth and on the details of the photometric noise, especially the level of correlated noise on the timescale of a transit. Most transit surveys show such red noise at levels of 3-6 mmag for untreated light curves, which can often be reduced to 1-2 mmag with decorrelation algorithms (Pont et al.

2007; Tamuz et al. 2005; Jenkins et al. 2000). As an example, the Monitor project shows red noise levels of 1-1.5 mmag (Irwin et al. 2007). The MEarth project’s employment of multiple telescopes may be a weapon against red noise if the systematics/correlated noise are largely independent from one telescope to another. Nevertheless, these considerations suggest that for transit depths less than ~ 5 mmag, MEarth may have to alert an outside observatory to achieve a very high significance transit detection.

3. Catalog of Potential M dwarf Targets

Despite their low intrinsic luminosities, M dwarfs are intrinsically abundant, and provide a bounty of bright survey targets. We have consulted the Lépine-Shara Proper Motion Catalog of northern stars (LSPM-North; Lépine & Shara 2005) for potential targets and their observational properties. LSPM-North is a nearly complete list of northern stars with proper motion greater than $0''.15 \text{ yr}^{-1}$. Lépine (2005) identifies a subsample of 2459 LSPM stars for which either trigonometric parallaxes or spectroscopic/photometric distance moduli indicate that their distance is less than 33 pc, as well as more than 1600 stars suspected to be dwarfs within 33 pc. Restricting to $d < 33$ pc keeps the rate of contamination from high proper motion subdwarfs small. At this distance, incompleteness is mainly due to the proper motion limit ($\mu > 0''.15 \text{ yr}^{-1}$).

LSPM gives V for stars with Tycho-2 magnitudes, and estimates V from USNO-B1.0 photographic magnitudes for the remaining stars. These magnitudes are supplemented with 2MASS JHK magnitudes. When there is a distance measurement in the literature, Lépine provides these (1676 with trigonometric parallaxes and 783 with spectroscopic/photometric distance moduli). For the remaining 1672 stars, Lépine estimates distance through a piecewise $V - J$ vs. M_V relationship which is calibrated by stars with known parallaxes. In assigning distances, we always use the value tabulated by Lépine, except for a small fraction of cases when the trigonometric parallax is uncertain by more than 15 %. In these cases we use Lépine’s piecewise $V - J$ vs. M_V relationship. We cull the Lépine (2005) subsample to probable M dwarfs by requiring $V - J > 2.3$, $J - K > 0.7$, $J - H > 0.15$ (motivated by Figures 28 and 29 in Lépine & Shara 2005). This leaves nearly 3300 probable nearby M, or late K, dwarfs. We hereafter refer to this culled sample of stars as the LSPM M dwarfs.

3.1. Estimating Stellar Parameters

We considered three routes towards estimating the luminosities, masses, and radii of the LSPM M dwarfs:

1. theoretical models of Baraffe et al. (1998), which offer synthetic $V - K$ colors that can then be matched to observed $V - K$ colors
2. empirically determined fits for the stellar parameters as a function of $V - K$ colors
3. the M_{\star} - M_K relations of Delfosse et al. (2000), combined with the empirical mass-radius relation of Bayless & Orosz (2006), and the bolometric corrections of Leggett et al. (2000).

The first method is problematic in that the theoretical models (not just those of Baraffe et al. 1998) are known to underestimate radii by 5-15 % for stars in the range $0.4 M_{\odot} \lesssim M \lesssim 0.8 M_{\odot}$ (Ribas 2006). Furthermore, as noted by Baraffe et al. (1998), the synthetic colors involving the V band are systematically too blue by ~ 0.5 mags, which is suggested to be due to some unmodeled source of V band opacity. While the second method avoids these problems, it suffers from significant dispersion in the stellar parameters for a given $V - K$ (see for example Figure 2 of Delfosse et al. 2000). When the absolute K magnitude, M_K , is well known, the third method does very well at estimating the mass and radius, relying on the small intrinsic scatter of the Delfosse and empirically determined mass-radius relations. However, only a third of the LSPM M dwarfs have trigonometric parallaxes, and the distance moduli for the remaining M dwarfs have uncertainties up to ± 0.6 mag. This uncertainty in distance propagates to a roughly $\pm 30\%$ uncertainty in mass, which is comparable to the scatter in the relations based on $V - K$ color. We settled on the third method, which at its worst produces errors comparable to the second method, while performing significantly better when the distance to the M dwarf is relatively well determined.

For each star, we insert the estimated M_K into the polynomial fit of Delfosse et al. (2000) to infer the mass. We then apply a polynomial fit to the mass-radius data of Ribas (2005) to convert this to a radius. To estimate the stellar luminosity, we adopt the bolometric corrections of Leggett (2000). Given this luminosity and radius, we estimate the T_{eff} , while we combine the mass and radius to estimate the star's $\log g$. The determined T_{eff} and $\log g$ drive our choice of synthetic spectra, as described below in §4.1.1.

In Table 1, we show a selection of adopted stellar parameters for different radius bins, along with approximate spectral types (calculated from the mean $V - K$ of each bin, and using Table 6 of Leggett 1992). We note that of all the estimated parameters, our calculations

below are most sensitive to the inferred radius. This is simply because the transit depth and hence the necessary photometric precision goes as R_\star^{-2} . We estimate the uncertainty in radius for individual determinations to be roughly 30-35 % (though better than 15% for the third of stars with trigonometric parallaxes), with this figure dominated by the uncertainty in distance modulus. Errors at this level are tolerable (as long as they are not significantly biased in one direction) and do not alter our conclusions.

4. Telescope Aperture Requirements

4.1. Photometric Precision

We follow standard calculations of photon, scintillation, and detector noise to simulate photometric precision for a variety of possible observational set-ups. The simulated systems described below are intended to be representative of commercially available CCDs and telescopes. We adopt the site characteristics of the Whipple Observatory on Mt. Hopkins, Arizona (altitude 2350 m) and the specifications of common semi-professional thinned, back-illuminated CCD detectors, but allow for other parameters, such as the aperture and filter to vary.

We calculate the precision as follows:

$$\text{precision} = \frac{\sqrt{N_\star + \sigma_{\text{scint}}^2 + n_{\text{pix}}(N_S + N_D + N_R^2)}}{N_\star} \quad (1)$$

where N_\star is the number of detected source photons, n_{pix} is the number of pixels in the photometric aperture, N_S is the number of photons per pixel from background or sky, N_D is the number of dark current electrons per pixel, and N_R is the RMS readout noise in electrons per pixel. We adopt the scintillation expression of Dravins et al. (1998)

$$\frac{\sigma_{\text{scint}}}{N_\star} = 0.09 \frac{X^{3/2}}{D^{2/3} \sqrt{2t}} \exp\left(-\frac{h}{8}\right) \quad (2)$$

where X gives the airmass (which we set at 1.5), D gives the aperture diameter in cm, t gives the exposure time in s, and h gives the observatory altitude above sea level in km.

For a common, commercially-packaged, Peltier-cooled CCD camera, $N_R = 10 \text{ e}^-/\text{pixel}$, and $N_D = 0.1 \text{ e}^-/\text{pixel/s}$, each of which are negligible for bright sources. To calculate n_{pix} we assume a circular photometric aperture of radius 5 ". For $13 \mu\text{m} \times 13 \mu\text{m}$ pixels, and a typical focal ratio of f/8, $n_{\text{pix}} = 62.9 * (D/30 \text{ cm})^2$.

We calibrated the sky background flux estimates ($\text{photons cm}^{-2} \text{ s}^{-1} \text{ arcsec}^{-2}$) for our simulated system using i and z band observations taken over several nights with KeplerCam

(see, e.g., Holman et al. 2007) and the 1.2 m telescope located at the Whipple Observatory. These measurements differ from what would be received by our hypothetical system by a factor of the overall throughput of the 1.2m system over the overall throughput of our system, in each bandpass of interest. We make a first order estimate of this ratio by using KeplerCam observations of stars with calibrated i and z magnitudes to determine the scale factor necessary for our simulated system to reproduce the number of counts received by KeplerCam. The sky background flux received by our hypothetical system is then approximately the observed flux divided by this scale factor. Of course, the actual sky background present in an exposure depends on many factors, in particular the phase of the moon and its proximity to the target object. For our calculations we take the median of our sky flux measurements. This estimate turns out to be an overestimate of the true median sky value because a disproportionate fraction of our observations were taken near full lunar phase.

We calculate N_\star with

$$N_\star = t \times \pi(D/2)^2 \times \int T(\lambda)f(\lambda)\frac{\lambda}{hc}d\lambda \quad (3)$$

where t is the exposure time, D is the aperture diameter, $f(\lambda)$ is the stellar flux described in §4.1.1 and $T(\lambda)$ is the overall system transmission described in §4.1.2.

In our calculation, we do not include the potentially significant noise from the intrinsic variability of the star. Though variability is common among M dwarfs, it is often on timescales different from the transit timescale or of a form distinct from a transit signal and thus removable. One common form of M dwarf variability is that of flares, which are easily distinguished from a transit in that flares result in an increase in flux as opposed to a decrement. Starspots are also a concern, but induce variability on a timescale defined by the stellar rotation period, which is much longer than that of a transit and hence may be distinguished. Because the M_{Earth} project is a targeted survey, troublesome variable M dwarfs could possibly be dropped in favor of photometrically quiet M dwarfs (such as the transiting-planet host GJ 436), though such variables might be worth retaining for non-transit related studies.

4.1.1. *Synthetic M dwarf Spectra*

We employ PHOENIX/NextGen model spectra (see Hauschildt, Allard, & Baron 1999 and references therein) to simulate the flux of our target M dwarfs. These model spectra have subsequently been updated with new TiO and H₂O line lists (Allard et al. 2000), which significantly improve M dwarf spectral energy distributions on the blue side of the optical. However, as pointed out by Knigge (2006), this improvement appears to be somewhat at

the expense of accuracy in $I - K$ colors, which the original NextGen models reproduce well. Given the importance of this spectral region for our studies, we exclusively use the original NextGen models.

The NextGen models are available over the range of M dwarf temperatures (2000 K to 4000 K), in steps of 100 K, for $4.0 \leq \log g \leq 5.5$ in steps of 0.5 dex, with $[\text{Fe}/\text{H}]=0$. For each star, we choose the spectrum with T_{eff} and $\log g$ most similar to the star’s inferred T_{eff} and $\log g$.

The synthetic spectra give the star’s surface flux, and therefore require a dilution factor, $x = (R_\star/d)^2$, to reproduce the flux incident on the Earth’s atmosphere. Since precise measurements of R_\star and d are not available for the M dwarf candidates, we instead calculate x by using observed magnitudes and scaling with respect to the zero magnitude fluxes. For example, we calculate the $V = 0$ dilution factor by equating $f(\lambda)_V = \int T_V(\lambda)f(\lambda)d\lambda / \int T_V(\lambda)d\lambda$ with the zero point $f(\lambda)_{V=0}$ taken from Bessell and Brett (1988), where T_V is the standard bandpass response of V (Bessell 1990, Bessell and Brett 1988).

If the photometric colors of the star match well with the colors of the synthetic spectrum, the dilution factor depends little on which band is chosen for the calculation. In practice, the synthetic and observed colors do not necessarily match up well. To more robustly estimate the dilution factor, we average the x ’s determined separately through the V, J , and K bands.

4.1.2. Transmission

With properly scaled synthetic spectra, we can simulate photometry for a rich variety of transmission functions. We perform our calculations for three scenarios: through the SDSS i and z filters (as defined by the transmission curves available from the SDSS DR1 webpage), and through a filter which cuts on and is open beyond ~ 700 nm, which we’ll refer to as the $i + z$ filter. For optical transmission, we take the square of the reflectivity curve (i.e. two mirror reflections) measured for a typical aluminum-coated mirror. To incorporate atmospheric transmission, we adopt the extinction coefficients of Hayes et al. (1975), determined by observation from the Mt. Hopkins Ridge (altitude 2350 m). For CCD response, we assume the quantum efficiency of a typical thinned, back illuminated CCD camera. Note that the overall system response beyond 800 nm is essentially set by the CCD. From our experience in trying to match simulated photon fluxes to actual observations of stars with known photometry, we find it prudent to adopt an additional overall transmission factor of 0.5. There are a variety of places where unaccounted for losses of transmission may creep in, e.g. when the QE, or mirror reflectivity do not meet the manufacturer’s

specifications. Note that we have neglected the reduction in collecting area due to a central obstruction (e.g. the secondary mirror), but this is more than accommodated for by our assumed loss factor. The overall system response through the $i + z$ filter is depicted in Fig 1, along with a $T_{\text{eff}} = 3000K$ synthetic M dwarf spectrum for comparison.

4.2. Precision and Aperture

In this section, we look at each of the LSPM M dwarfs, and ask what is the necessary telescope aperture diameter to achieve a desired precision in a fixed exposure time. In this section, we fix the exposure time to 150 seconds, an arbitrarily chosen exposure time but useful for comparing necessary apertures (later we allow the exposure time to vary). We also set the desired precision to that which is necessary for a 3 sigma detection, per measurement, of the transit of a $2-R_{\oplus}$ planet. Note that the required precision then varies for each of the stars, as a function of the estimated stellar radius. For a $0.33-R_{\odot}$ M dwarf, a 3 sigma detection requires a precision of 0.001, but for a $0.10-R_{\odot}$ M dwarf, it corresponds to a precision of only 0.011.

With this varying precision and fixed exposure time, we have calculated the necessary aperture for each of the LSPM M dwarfs through the z and $i + z$ filters. In Figure 2 we display the cumulative distribution of LSPM M dwarfs as a function of aperture for the z and $i + z$ cases. In comparison to the z filter (dot-dashed curve), it is apparent that using the $i + z$ filter (dashed curve) significantly increases the fraction of stars that meet the desired precision in 150 s. This is particularly important for apertures in the range 35-40 cm, where use of $i + z$ more than doubles the number of stars meeting the precision requirements.

This calculation also drives home a very important point: even though late M dwarfs are intrinsically less luminous, and on the mean, fainter than earlier M dwarfs, this is more than compensated by the relaxed precision requirements that accompany their smaller radii. In fact, the stars with the smallest necessary aperture are dominated by late M dwarfs. In Figure 2 we have overplotted (solid curve) the cumulative distribution of stars with estimated radii $< 0.33 R_{\odot}$ (N=1976) as a function of necessary aperture through the $i + z$ band. This selection of stars is motivated by the practical difficulty of achieving a precision better than 0.001 from the ground, which corresponds to the 3 sigma precision of $2-R_{\oplus}$ planet transiting a $0.33-R_{\odot}$ star. One can see that the aperture requirements for these stars are quite favorable; 80 % of the sample can be observed at the requisite precision in 150 s integrations with telescopes of aperture 40 cm.

5. Field of View Requirements

Since we target only one star per field, the required size of the field of view (FOV) is defined by the need to have an adequate number of calibrating stars. For each field, we require the number of photons received from calibrating stars to be 10 times the number of photons received from the target M dwarf. We further require that each calibrating star be between 0.2 and 1.2 times the brightness of the target star. Note that these requirements are relatively strict to give tolerance for the possibility of variables or other unsuitable stars being among the calibrators. For each LSPM M dwarf, we determine the size of the smallest square box (centered on the M dwarf) that meets the calibration requirements.

For this calculation, we query the 2MASS Point Source Catalog (Cutri et al. 2003), using WCSTools (Mink 1998) around the position of each M dwarf. This query results in a list of potential calibrating stars. For each of these potential calibrators, we transform from 2MASS J and K_s magnitudes into estimates of i and z magnitudes. This transformation is necessary since the calibrator stars do not, in general, lie in fields covered by the SDSS survey, and in cases where they do, the SDSS photometry is usually saturated. The transformation relies on a polynomial fit to $i - J$ as a function of $J - K_s$ as we now detail. Our dataset for the transformation is a sample of cross-matched stars in 2MASS and the SDSS Photometric Data Release 5 (Adelman-McCarthy & et al. 2007) from an arbitrarily chosen 3° by 3° field covered by the SDSS DR5 dataset. SDSS photometry was accepted if not flagged as SATURATED, EDGE, DEBLENDED_AS_MOVING, CHILD, INTERP_CENTER, or BLENDED.

We derived a quadratic fit to $i - J$ and a linear function fit to $z - J$, each as a function of $J - K_s$. The resulting fits, displayed in Figure 3, are:

$$i - J = 1.09 - 1.46 * (J - K_s) + 2.50 * (J - K_s)^2 \quad 0.2 < J - K_s < 0.9 \quad (4)$$

$$z - J = 0.56 + 0.73 * (J - K_s) \quad 0.2 < J - K_s < 0.9 \quad (5)$$

For the primary M dwarfs, $J - K_s$ is degenerate, so we rely instead on the M_J vs. $i - J$ and M_J versus $z - J$ relations of Hawley et al. (2002). The uncertainty in M_J reaches ± 0.6 mag (dominated by the uncertainty in distance), but leads to a much smaller uncertainty in $i - J$ (< 0.3 mag) and $z - J$ (< 0.2 mag) because of the small dynamic range of these colors over the M dwarf sequence.

We estimate the ratio of photon fluxes in each band by $10^{-0.4\Delta i}$ or $10^{-0.4\Delta z}$, where Δi , Δz are the differences in i, z magnitude between target and calibrator. To compare photon fluxes through different bands, one must of course take into account the difference in relative throughput between each band. For these quick estimates, we account for the relative throughput of i vs. z via the Q factor described in Fukugita et al. (1996). To illustrate, a

source with equal i and z magnitudes will have approximately Q_i/Q_z (≈ 2) more photons through the i band than through the z band. With estimates for the relative number of photons in the calibrators now in hand, we place successively larger boxes around the target M dwarf, until the calibration requirement is met. In Figure 4, we show the cumulative distribution of all LSPM M dwarfs as a function of the required FOV for both the z filter (dot-dashed), and $i + z$ filter (dashed).

Some key points arise from this investigation. An unsurprising one is that brighter targets require significantly larger fields than fainter targets, due simply to the relative sparseness of brighter calibrators. Another is that using an $i + z$ filter (rather than z alone) saves somewhat on the field of view. This is again unsurprising since cutting on at a bluer wavelength increases the relative number of photons from generally bluer calibrators. Note that although the use of the $i + z$ filter adds to the number of M dwarfs observable by our criteria, it may complicate calibration. Fringing, for example, may be an issue in this bandpass with a thinned, back-illuminated CCD. We expect however, that the situation will not be too different from the z band observing experiences of Holman et al. (2007), where fringing was apparent, but had little effect on the photometric precision. In addition, the generally bluer comparison stars may introduce calibration issues. We expect that this too will be surmountable, for example, through the use of color-dependent extinction corrections.

The relative faintness of late M dwarfs emerges as a very favorable characteristic in this calculation. In Figure 4, we have included the cumulative distribution for the subset of LSPM M dwarfs with estimated radius $< 0.33 R_\odot$ (solid curve) for $i + z$. This is the same subset of stars motivated by aperture considerations and described in §4.2.

The propitious aspects of these late M dwarfs that arise in both aperture and FOV considerations are worthy of further investigation. In Figure 5, we have plotted the necessary aperture versus necessary field of view for each of the LSPM M dwarfs, with stars of radius $< 0.33 R_\odot$ represented by filled circles, and stars of radius $> 0.33 R_\odot$ by open circles. The criteria for calibrators, photometric precision, and exposure time are again as described above. We see that the late M dwarfs occupy a locus in aperture-FOV space that is very fortunate from an instrumental design standpoint.

6. Survey Duration and Number of Telescopes

In this section we estimate the amount of telescope time necessary for a successful MEarth Project. Our conclusion is framed in units of *telescope-years*, reflecting the fact that the survey duration and the number of telescopes is a trade-off. Our calculation is tailored

to the characteristics of $2\text{-}R_{\oplus}$ -sized planets orbiting in the habitable zones of the host stars.

The outline of the calculation is as follows. We first determine the fraction of a telescope’s time, f_{tel} that must be devoted to each star to guarantee the temporal coverage necessary for catching transits of habitable zone planets. We then calculate the number of observing nights, N_{nights} , that are necessary until one can be 90 % confident that at least one transit would have fallen during an observation session. The effective number of telescope nights, N_{eff} is then $N_{\text{eff}} = N_{\text{nights}} \times f_{\text{tel}}$. The total effective number of telescope nights is determined by calculating and summing N_{eff} over the list of stars to survey.

The calculation of f_{tel} is done as follows: 1) For each star, and for a given aperture, we determine the necessary exposure time to achieve a 3 sigma detection of a $2 R_{\oplus}$ planet. In addition, we assume an overhead time of 60 s to account for time spent slewing between targets. 2) We determine the transit duration using the inferred stellar parameters from section 3. We assume a circular orbit at a distance from the star for which the planet receives the same stellar flux as the Earth. We further assume a mid-latitude transit, which leads to a transit duration of 0.866 times that of an equatorial transit. 3) We require at least 2 visits to the star per transit duration. This then sets the cadence to $2/\text{transit duration}$ (cycles per unit time). We impose a minimum cadence of one visit per 60 minutes, to ensure that we have sufficient temporal coverage to catch shorter transit duration planets (i.e. planets interior of the habitable zone). 4) Finally, the f_{tel} dedicated to a given star is given by $f_{\text{tel}} = \text{cadence} \times (\text{exposure time} + \text{overhead})$. In the top panel of Figure 6, we display a histogram of the sample of 1,976 late M dwarfs, binned by f_{tel} . These histograms give a sense of what fraction of a telescope’s time must be devoted to individual M dwarfs, when those stars are being actively observed. f_{tel} is calculated as described above for aperture diameters of 20 cm (dashed), 35 cm (dotted), and 50 cm (solid). One can see that for 20 cm apertures, a significant fraction of stars would require more than 10 % of the telescope’s time while actively being observed. For 35 and 50 cm apertures, a typical star requires $\sim 5\%$ and $\sim 3\%$, respectively, of a telescope’s time.

Our calculation for N_{nights} involves simulations similar to those performed in ‘window function’ calculations that are common in the literature (see, for example, Pepper et al 2005). The major difference is that here we require only one transit. This is justified because we anticipate reducing photometry in real-time, so that transits events can identified and confirmed while still in progress. We inject transit signals over an extensive grid of possible phases, with periods assigned to each star corresponding to planets in habitable zone orbits. For the purposes of simulation, we assume observational seasons of 60 nights with 9 hours of observing each night. We randomly knock out 50 % of observing nights to account for weather effects. In practice, most stars in the sample are visible from Mt. Hopkins (latitude

31.6° N) for more than 60 nights each year (neglecting weather) and are visible for less than 9 hours each night, but $9 \text{ hours} \times 60$ roughly represents the number of hours a typical star is visible over the course of a season. To avoid skewed results from periods near integer or half-integer number of days (which are known to show resonances in detection probability), we simulate over a uniform range of possible periods for each star. The upper end of this range of periods is defined by planets receiving the same stellar flux as Earth, and at the lower end by planets with an equilibrium temperature of 290 K (assuming a wavelength-integrated Bond albedo of 0.3). We determine N_{nights} by requiring that 90 % of transit signals are recovered. In the bottom panel of Figure 6, we give a histogram for the total number of nights during which each star must be observed.

The only remaining issue is to select which M dwarfs to sum N_{eff} over. The stars with the optimal N_{eff} are the coolest M dwarfs, for which the periods of habitable zone orbits are shortest. The previously described sample of 1,976 late M dwarfs with radius $< 0.33R_{\odot}$ are once again very appropriate under this consideration. In Figure 7, we have summed N_{eff} over these M dwarfs as a function of aperture. The effect of increasing the aperture size is to decrease the integration times required to each star, and hence to decrease the fraction of its time that a telescope must devote to each star. At $\sim 30 \text{ cm}$, the marginal benefit of adding more aperture diminishes, simply because at this aperture, overhead time spent slewing between targets begins to dominate over the actual time spent integrating on targets.

At 30 cm, $N_{\text{eff}}=22.1$ telescope-years. Thus ten such telescopes could survey the sample of 1,976 late M dwarfs in 2.2 years. Note that simply adding more telescopes to the network does not necessarily reduce the survey completion time. For example a significant fraction of the stars in the late M dwarf sample require a time baseline of more than 90 nights to achieve 90 % confidence that a transit event would have occurred during an observational session (see Figure 6). If many of these stars are only visible 30 good weather nights a year, then observations of these stars must be spread out over 3 years, regardless of the amount of telescope time one devotes to each star.

7. Conclusions and Discussion

We have investigated the design requirements for the MEarth Project, a survey conceived to monitor Northern Hemisphere M dwarfs for transits of habitable planets, with a sensitivity to detect planets down to a radius of $2R_{\oplus}$. In our investigation, 1,976 late M dwarfs ($R < 0.33R_{\odot}$) emerged as the most favorable survey targets, initially for reasons related to photometric precision. Despite their relative faintness, it is easier to achieve the required sensitivity to detect a given planet because their small radii lead to deep transit

signals. In consideration of the required field-of-view, late M dwarfs once again arose as the most favorable survey targets—in this case *because* of their relative faintness. A final investigation into the amount of telescope time required to achieve transit detections of habitable planets again favored late M dwarfs, because of the short periods of habitable zone orbits.

Because of the increased geometric probability of transit for habitable planets around the late M dwarfs, the constraints on the occurrence rate of such planets are correspondingly tighter. We can perform an ex post facto analysis on the sample of 1,976 late M dwarfs with an estimated $R < 0.33R_{\odot}$, using their individual inferred stellar radii and the estimated semi-major axes of planets in their habitable zones, and assuming a recovery rate of 90 % for planets transiting from the habitable zone. For this sample of stars, a lack of any transit detections of habitable planets would lead to an upper limit (99 % confidence) of 17 % for the occurrence of such planets. For a true occurrence rate of 10 % for habitable planets (larger than $2 R_{\oplus}$), the expected yield would be 2.6 such planets. We note that for even closer planets, such as the hot Neptune transiting GJ 436, the expected yield is significantly larger, and thus, in their own right could justify a project to monitor this many M dwarfs. We also note that our sample of M dwarfs include 450 stars with an estimated $R < 0.17R_{\odot}$, to which the MEarth network could be sensitive to transiting planets as small as $1 R_{\oplus}$. To achieve this sensitivity, the exposure times for these 450 stars would need to be increased by roughly a factor of 4 compared to the exposure times calculated in this paper.

Once built, the MEarth network of robotic telescopes will be able to survey the 1,976 late M dwarfs in 22 telescope-years, if equipped with 30 cm aperture telescopes, using the ‘i+z’ filter described in section 4. From an instrumental viewpoint, successfully observing this sample of M dwarfs is challenged by the ~ 10 % of this sample (see Figure 4) for which the estimated field of view requirements are greater than 30 arcmin by 30 arcmin. Possible solutions to this challenge worth exploring include, for example, the addition of a wide angle-node to the MEarth network, or simply using a large-format camera. It may also be possible to accommodate these stars by using custom field orientations in order to grab extra calibrating stars, or to relax the conservative calibrating criteria that we assumed in our field of view calculations.

This study has confirmed the status of nearby late M dwarfs as bearers of the lowest hanging fruit in the search for habitable rocky planets. Excitingly, these stars remain largely unexplored: Since late M dwarfs are very faint at the visible wavelengths at which iodine provides reference lines, they are not accessible to current radial velocity planet searches. Besides the search for transiting planets, a plan to photometrically monitor this many M dwarfs represents a large step forward in the study of the intrinsic variability, and long-term activity of M dwarfs. The identification and monitoring of spotted stars,

for example, will be useful to future, near IR radial velocity observational programs which will be compromised by the radial velocity jitter and spurious signals that might result.

We gratefully acknowledge funding for this project from the David and Lucile Packard Fellowship for Science and Engineering. We would like to thank Andrew Szentgyorgyi, David Latham, Matt Holman and Cullen Blake for helpful comments, and an anonymous referee for thoughtful comments and helpful recommendations. This publication makes use of data products from the Two Micron All Sky Survey, which is a joint project of the University of Massachusetts and the Infrared Processing and Analysis Center/California Institute of Technology, funded by the National Aeronautics and Space Administration and the National Science Foundation.

REFERENCES

- Adelman-McCarthy, J. K. & et al. 2007, VizieR Online Data Catalog, 2276, 0
- Aigrain, S., & Pont, F. 2007, MNRAS, 378, 741
- Allard, F., Hauschildt, P. H., & Schwenke, D. 2000, ApJ, 540, 1005
- Alonso, R., Brown, T. M., Torres, G., Latham, D. W., Sozzetti, A., Mandushev, G., Belmonte, J. A., Charbonneau, D., & et al. 2004, ApJ, 613, L153
- Baglin, A. 2003, Advances in Space Research, 31, 345
- Bakos, G., Noyes, R. W., Kovács, G., Stanek, K. Z., Sasselov, D. D., & Domsa, I. 2004, PASP, 116, 266
- Baraffe, I., Chabrier, G., Allard, F., & Hauschildt, P. H. 1998, A&A, 337, 403
- Barman, T. 2007, ApJ, 661, L191
- Bayless, A. J. & Orosz, J. A. 2006, ApJ, 651, 1155
- Beaulieu, J. P., Bennett, D. P., Fouqué, P., Williams, A., Dominik, M., Jorgensen, U. G., Kubas, D., Cassan, A., & et al. 2006, Nature, 439, 437
- Borucki, W. J., Koch, D., Basri, G., Brown, T., Caldwell, D., Devore, E., Dunham, E., Gautier, & et al. 2003, in ESA Special Publication, Vol. 539, ESA Special Publication, ed. M. Fridlund, T. Henning, & H. Lacoste, 69

- Charbonneau, D., Allen, L. E., Megeath, S. T., Torres, G., Alonso, R., Brown, T. M., Gilliland, R. L., Latham, D. W., Mandushev, G., O'Donovan, F. T., & Sozzetti, A. 2005, *ApJ*, 626, 523
- Charbonneau, D., Brown, T. M., Burrows, A., & Laughlin, G. 2007, in *Protostars and Planets V*, ed. B. Reipurth, D. Jewitt, & K. Keil, 701
- Charbonneau, D., Brown, T. M., Noyes, R. W., & Gilliland, R. L. 2002, *ApJ*, 568, 377
- Charbonneau, D., & Deming, D. 2007, *ArXiv e-prints*, 706, arXiv:0706.1047
- Christian, D. J., Pollacco, D. L., Clarkson, W. I., Collier Cameron, A., Evans, N., Fitzsimmons, A., Haswell, C. A., Hellier, C., & et al. 2005, in *ESA Special Publication*, Vol. 560, *ESA Special Publication*, ed. F. Favata & et al., 475
- Cowan, N. B., Agol, E., & Charbonneau, D. 2007, *MNRAS*
- Cutri, R. M., Skrutskie, M. F., van Dyk, S., Beichman, C. A., Carpenter, J. M., Chester, T., Cambresy, L., Evans, T., & et al., N. 2003, *2MASS All Sky Catalog of point sources*.
- Deeg, H. J. 2004, *Stellar Structure and Habitable Planet Finding*, 538, 231
- Delfosse, X., Forveille, T., Ségransan, D., Beuzit, J.-L., Udry, S., Perrier, C., & Mayor, M. 2000, *A&A*, 364, 217
- Deming, D., Seager, S., Richardson, L. J., & Harrington, J. 2005, *Nature*, 434, 740
- Deming, D., Harrington, J., Seager, S., & Richardson, L. J. 2006, *ApJ*, 644, 560
- Deming, D., Harrington, J., Laughlin, G., Seager, S., Navarro, S. B., Bowman, W. C., & Horning, K. 2007, *ArXiv e-prints*, 707, arXiv:0707.2778
- Dravins, D., Lindegren, L., Mezey, E., & Young, A. T. 1998, *PASP*, 110, 610
- Fukugita, M., Ichikawa, T., Gunn, J. E., Doi, M., Shimasaku, K., & Schneider, D. P. 1996, *AJ*, 111, 1748
- Gillon, M., Courbin, F., Magain, P., & Borguet, B. 2005, *A&A*, 442, 731
- Gillon, M., et al. 2007, *A&A*, 472, L13
- Gould, A., Pepper, J., & DePoy, D. L. 2003, *ApJ*, 594, 533
- Grillmair, C. J., Charbonneau, D., Burrows, A., Armus, L., Stauffer, J., Meadows, V., Van Cleve, J., & Levine, D. 2007, *ApJ*, 658, L115

- Harrington, J., Hansen, B. M., Luszcz, S. H., Seager, S., Deming, D., Menou, K., Cho, J. Y. K., & Richardson, L. J. 2006, *Science*, 314, 623
- Harrington, J., Luszcz, S., Seager, S., Deming, D., & Richardson, L. J. 2007, *Nature*, 447, 691
- Hauschildt, P. H., Allard, F., & Baron, E. 1999, *ApJ*, 512, 377
- Hawley, S. L., Covey, K. R., Knapp, G. R., Golimowski, D. A., Fan, X., Anderson, S. F., Gunn, J. E., Harris, H. C., & et al. 2002, *AJ*, 123, 3409
- Hayes, D. S., Latham, D. W., & Hayes, S. H. 1975, *ApJ*, 197, 587
- Holman, M. J., et al. 2007, *ApJ*, 664, 1185
- Irwin, J., Irwin, M., Aigrain, S., Hodgkin, S., Hebb, L., & Moraux, E. 2007, *MNRAS*, 375, 1449
- Jenkins, J. M., Witteborn, F., Koch, D. G., Dunham, E. W., Borucki, W. J., Updike, T. F., Skinner, M. A., & Jordan, S. P. 2000, *Proc. SPIE*, 4013, 520
- Knigge, C. 2006, *MNRAS*, 373, 484
- Knutson, H. A., Charbonneau, D., Allen, L. E., Fortney, J. J., Agol, E., Cowan, N. B., Showman, A. P., Cooper, C. S., & Megeath, S. T. 2007, *Nature*, 447, 183
- Leggett, S. K., Allard, F., Dahn, C., Hauschildt, P. H., Kerr, T. H., & Rayner, J. 2000, *ApJ*, 535, 965
- Lépine, S. 2005, *AJ*, 130, 1680
- Lépine, S. & Shara, M. M. 2005, *AJ*, 129, 1483
- Mandushev, G., Torres, G., Latham, D. W., Charbonneau, D., Alonso, R., White, R. J., Stefanik, R. P., & et al. 2005, *ApJ*, 621, 1061
- McCullough, P. R., Stys, J. E., Valenti, J. A., Fleming, S. W., Janes, K. A., & Heasley, J. N. 2005, *PASP*, 117, 783
- McCullough, P. R., & Burke, C. J. 2007, *Transiting Extrapolar Planets Workshop*, 366, 70
- Mink, D. J. 1998, in *Bulletin of the American Astronomical Society*, Vol. 30, 1144

- O'Donovan, F. T., Charbonneau, D., Torres, G., Mandushev, G., Dunham, E. W., Latham, D. W., Alonso, R., Brown, T. M., Esquerdo, G. A., Everett, M. E., & Creevey, O. L. 2006, *ApJ*, 644, 1237
- Pepper, J., & Gaudi, B. S. 2005, *ApJ*, 631, 581
- Pollacco, D., et al. 2006, *Ap&SS*, 304, 253
- Pont, F., Zucker, S., & Queloz, D. 2006, *MNRAS*, 373, 231
- Pont, F., et al. 2007, *Transiting Extrapolar Planets Workshop*, 366, 3
- Ribas, I. 2006, *Astrophysics and Space Science*, 304, 89
- Richardson, L. J., Deming, D., Horning, K., Seager, S., & Harrington, J. 2007, *Nature*, 445, 892
- Scalo, J., et al. 2007, *Astrobiology*, 7, 85
- Seager, S., Kuchner, M., Hier-Majumber, C., & Militzer, B. 2007, *ArXiv e-prints*, 707, arXiv:0707.2895
- Tamuz, O., Mazeh, T., & Zucker, S. 2005, *MNRAS*, 356, 1466
- Tarter, J. C., Backus, P. R., Mancinelli, R. L., Aurnou, J. M., Backman, D. E., Basri, G. S., Boss, A. P., Clarke, A., & et al. 2007, *Astrobiology*, 7, 30
- Tinetti, G., et al. 2007, *Nature*, 448, 169
- Udry, S., et al. 2007, *A&A*, 469, L43
- Valencia, D., Sasselov, D. D., & O'Connell, R. J. 2007, *ApJ*, 656, 545
- Vidal-Madjar, A., Lecavelier des Etangs, A., Désert, J.-M., Ballester, G. E., Ferlet, R., Hébrard, G., & Mayor, M. 2003, *Nature*, 422, 143

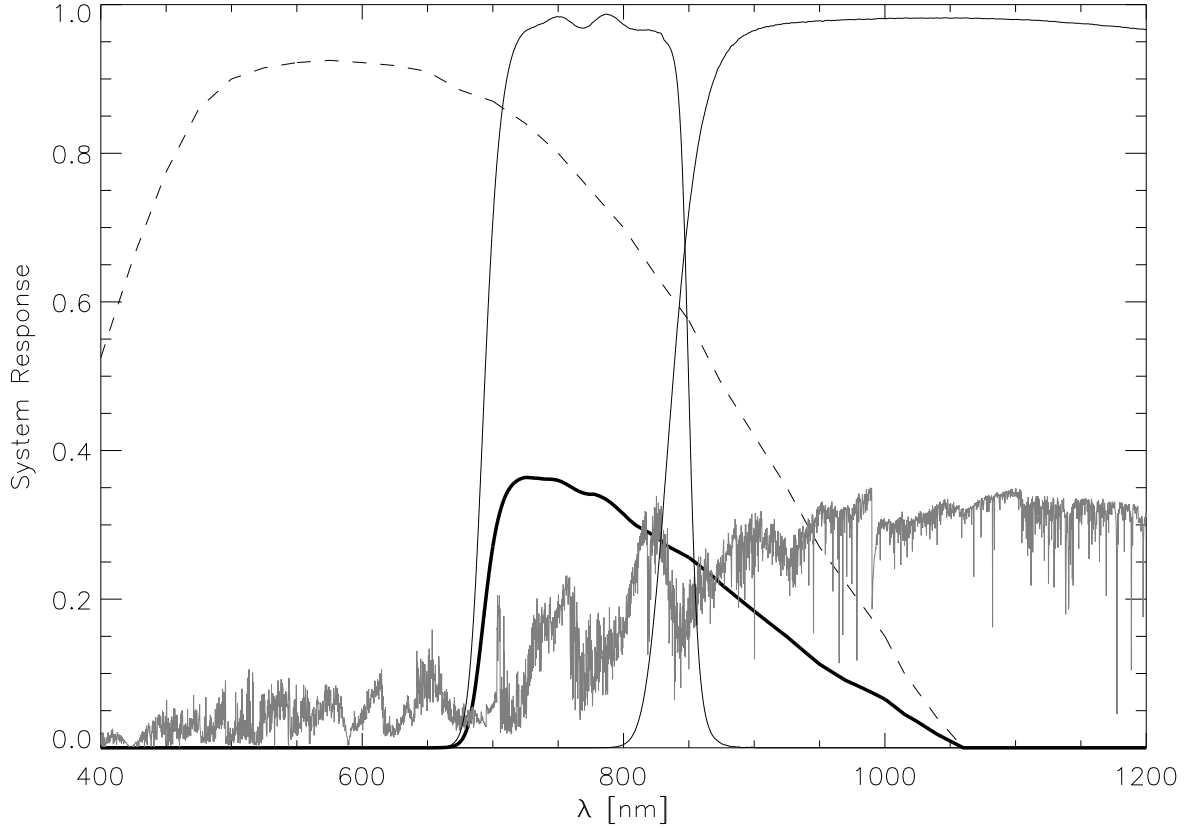


Fig. 1.— The overall system response (thick black) through the $i + z$ filter, incorporating atmospheric extinction, CCD quantum efficiency, mirror reflectivity, and an overall 50 % throughput loss. At long wavelengths, the system response is dominated by the CCD quantum efficiency (dashed). For comparison, we show the transmission curves of SDSS i and z filters. In gray, a NextGen M dwarf spectrum with $T_{\text{eff}} = 3000$ K, scaled for clarity.

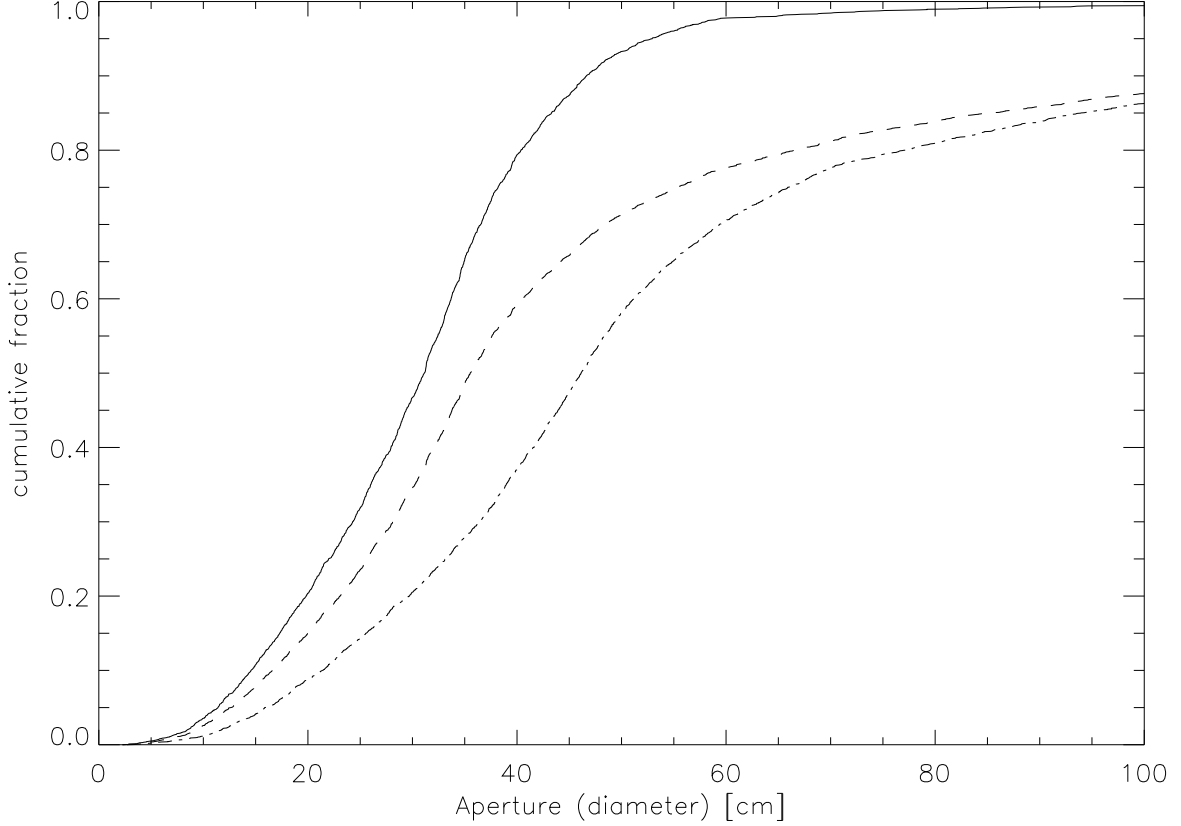


Fig. 2.— Cumulative distribution of LSPM M dwarfs as a function of aperture. The aperture is that necessary for achieving, in a 150 second integration, the requisite sensitivity for a 3 sigma detection of a $2-R_{\oplus}$ planet. Note that the required sensitivity varies from M dwarf to M dwarf as a function of stellar radius. The dot-dashed curve is for a calculation through the z filter, while the dashed curve is for the $i+z$. The solid curve is for a subset of LSPM M dwarfs with estimated radii $< 0.33R_{\odot}$ ($i+z$ filter).

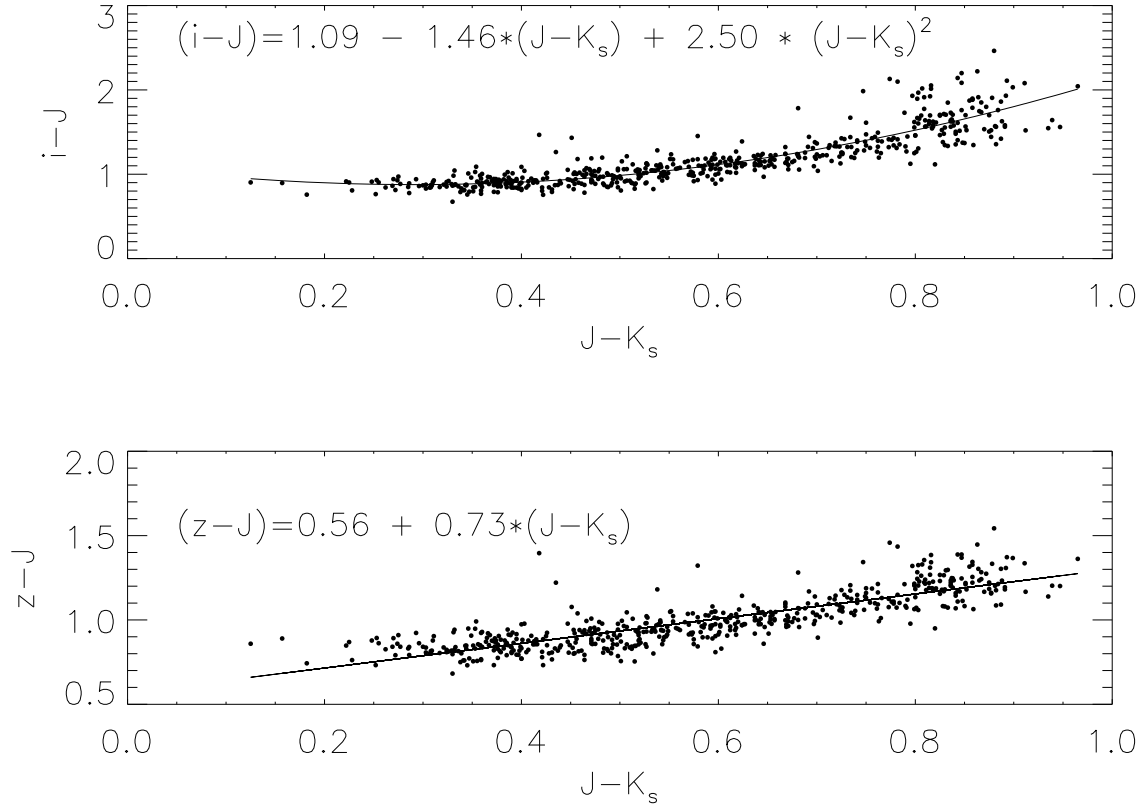


Fig. 3.— Transformation from J and K_s to i (top panel) and z (bottom panel). Each point represents a star that has been cross-matched in the 2MASS and SDSS surveys from an arbitrarily chosen field covered by the SDSS DR5 dataset. The displayed best-fit curves and corresponding equations are determined by a least squares fit to these data.

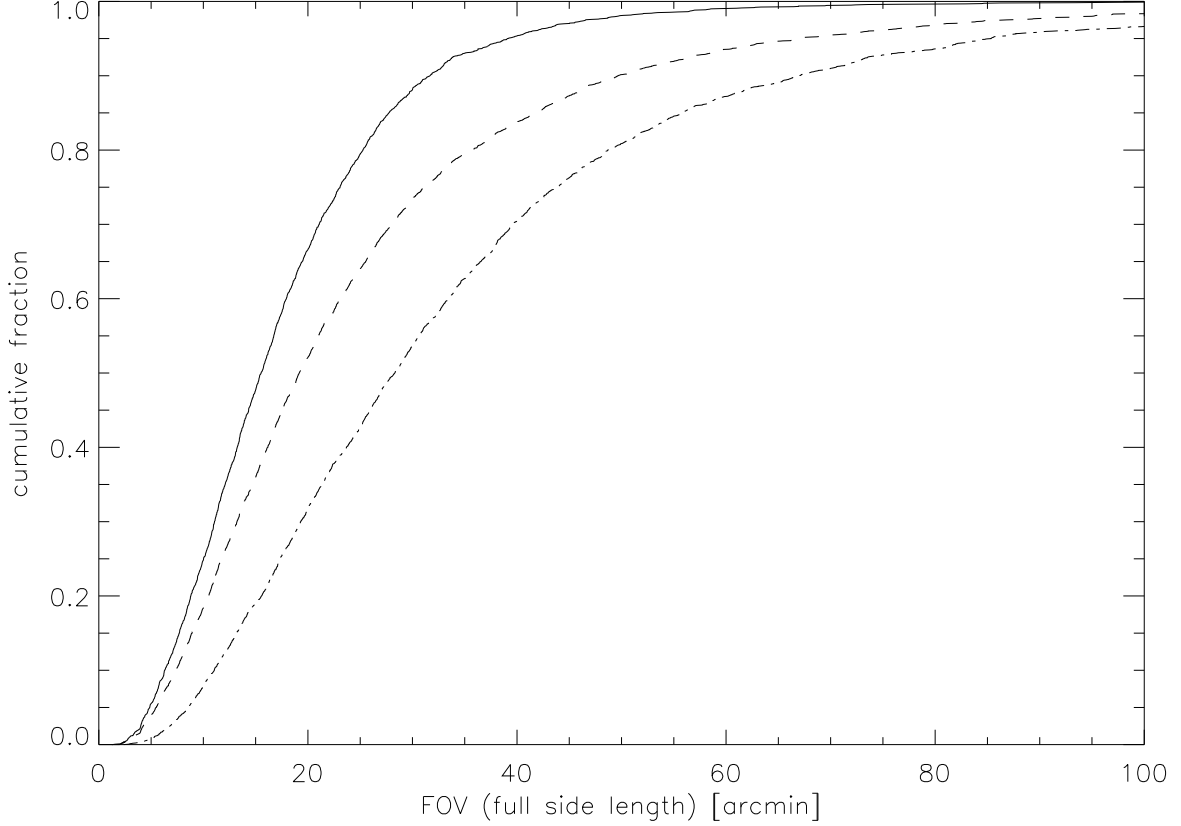


Fig. 4.— Cumulative distribution of LSPM M dwarfs as a function of the necessary field of view, where we require that the field includes ten times the photon flux from calibrator stars than from the target M dwarf. The required FOV is determined on a star-by-star basis by querying 2MASS for appropriate calibrating stars around the position of each target M dwarf. The dot-dashed curve is for a calculation through the z filter, while the dashed curve is for the $i + z$. The solid curve is for a subset of LSPM M dwarfs with estimated radii $< 0.33R_{\odot}$ ($i + z$ filter).

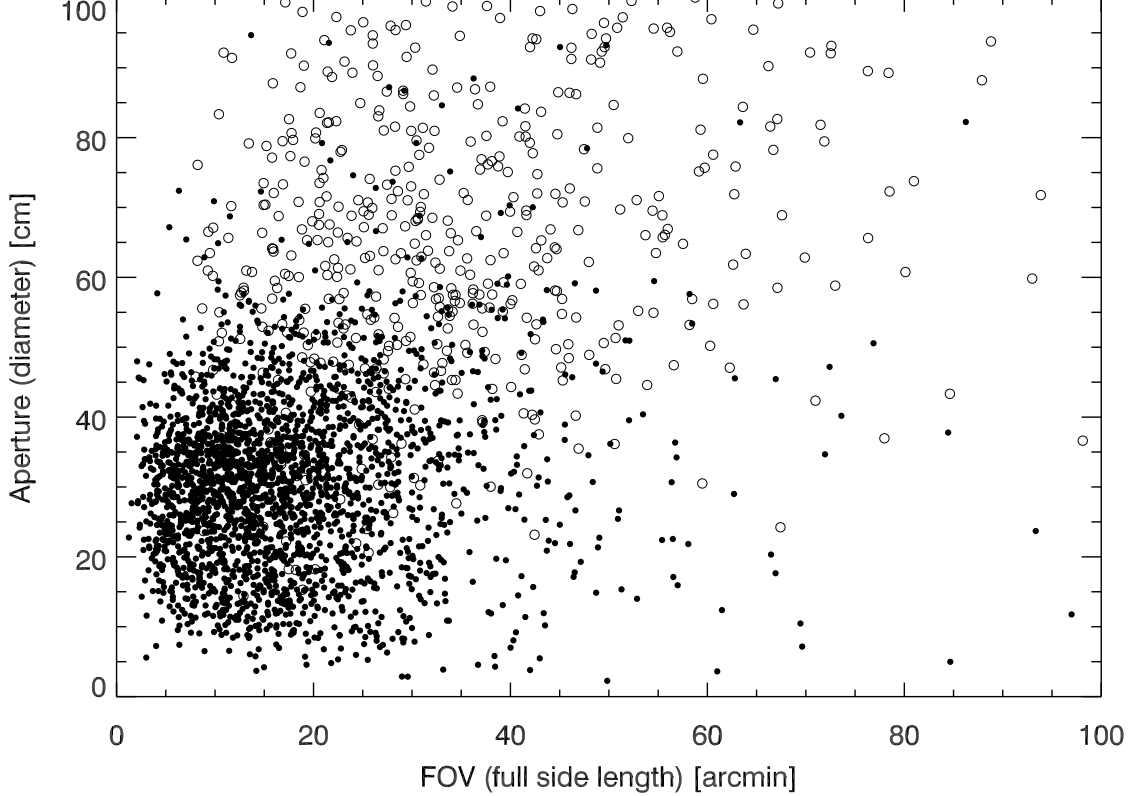


Fig. 5.— Necessary aperture vs. necessary FOV for LSPM M dwarfs. Stars with radius $> 0.33 R_{\odot}$ are represented by open circles, while stars with radius $< 0.33 R_{\odot}$ are represented by filled circles. The required precision (for aperture calculation) is that necessary to achieve a 3 sigma detection of a transiting $2 R_{\oplus}$ planet in a 150 second integration through the $i+z$ filter. The range of the x and y axes match that of the radius $< 0.33 R_{\odot}$ stars, while 30 % of the radius $> 0.33 R_{\odot}$ M dwarfs require more than a 100 cm aperture, and thus fall above the plot limits.

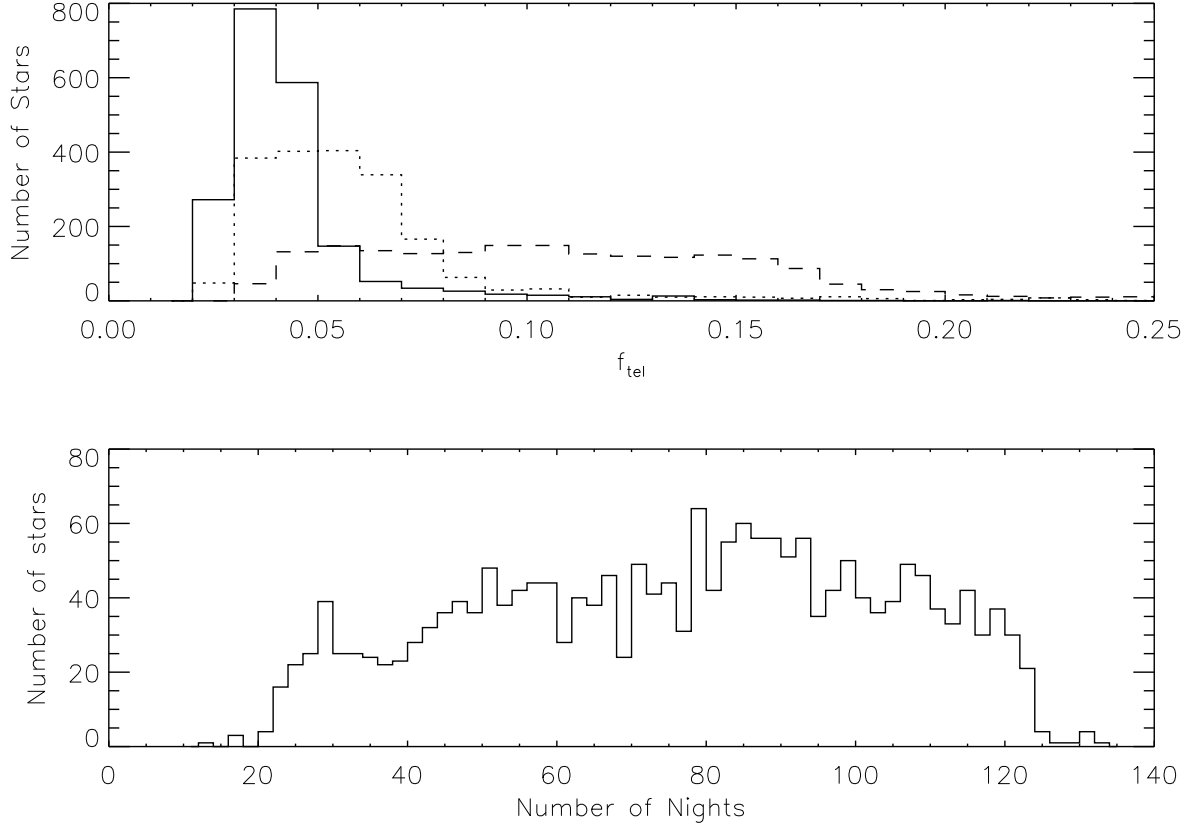


Fig. 6.— *Top:* Histogram of the late M dwarf sample, binned by f_{tel} , the fraction of telescope's time devoted to the star. The dashed curve give results for 20 cm aperture, dotted for 35 cm, and solid for 50 cm. *Bottom:* Histogram of the late M dwarf sample, binned by N_{nights} , the number of observing nights required to be 90 % confident that at least one transit event from a habitable zone-orbiting planet would have fallen during an observational session.

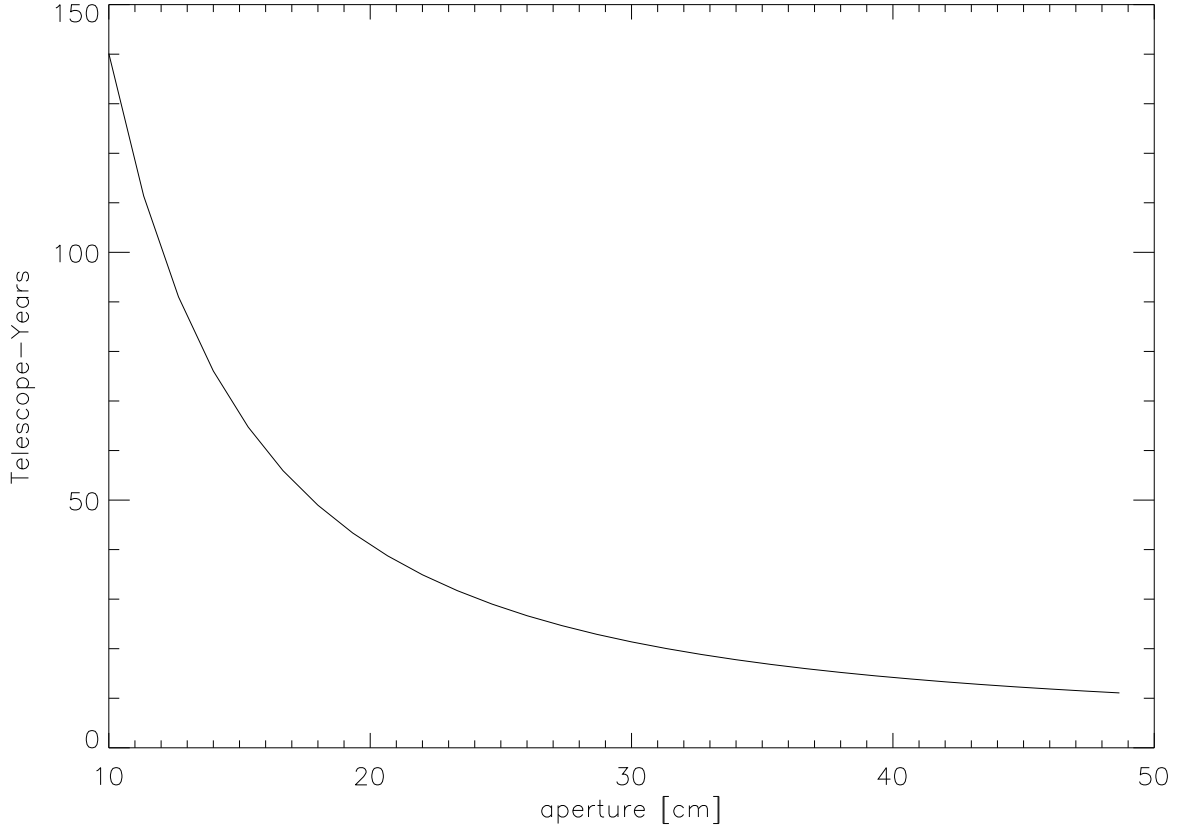


Fig. 7.— Number of telescope-years required to survey the sample of 1,976 late M dwarfs, as a function of aperture. This is calculated by summing $f_{\text{tel}} \times N_{\text{nights}}$ over each M dwarf, where f_{tel} is the fraction of telescope’s time devoted to the star, and N_{nights} is the number of observing nights required to be 90 % confident that at least one transit event from a habitable zone-orbiting planet would have fallen during an observational session.

Table 1. LSPM M dwarf Parameters^a

Sp. Type ^b	N	$R [R_{\odot}]$	$M [M_{\odot}]$	J
M0	129	.69	.68	7.58
M1	128	.62	.61	7.80
M2	225	.55	.54	8.10
M3	419	.44	.43	8.64
M4	890	.33	.32	9.44
M5	1043	.24	.22	10.21
M6	348	.15	.13	11.15
M7 & M8	114	.12	.09	12.06

^aMean Values for different radius bins

^bSpectral type estimated by a fit to Leggett (2000) data as function of $V - K$ color.